First publ. in: International Journal of Cancer ; 130 (2012), 7. - pp. 1544-1557

http://dx.doi.org/10.1002/ijc.26149

Analysis of the cellular uptake and nuclear delivery of insulin-like growth factor binding protein-3 in human osteosarcoma cells

Lucia Micutkova[1], Martin Hermann[2], Martin Offterdinger[3], Michael W. Hess[4], Andrea Matscheski[1], Haymo Pircher[1], Christoph Mück[1], Hannes-Leonhard Ebner[4], Andreas Laich[1], Elisa Ferrando-May[5], Werner Zwerschke[1], Lukas A. Huber[6] and Pidder Jansen-Dürr[1]

[1] Institute for Biomedical Aging Research, Austrian Academy of Sciences, Rennweg 10, A-6020 Innsbruck, Austria

[2] Department of Visceral, Transplant and Thoracic Surgery, KMT Laboratory, Center of Operative Medicine, Innsbruck Medical University, Innrain 66, A-6020 Innsbruck, Austria

[3] Division of Neurobiochemistry/Biooptics, Biocenter, Innsbruck Medical University, Fritz-Pregl-Str. 3, A-6020 Innsbruck, Austria

[4] Division of Histology and Embryology, Innsbruck Medical University, Müllerstrasse 59, A-6020 Innsbruck, Austria

[5] University of Konstanz Bioimaging Center, P.O. 604, D-78457 Konstanz, Germany

[6] Division of Cell Biology, Biocenter, Innsbruck Medical University, Fritz-Pregl-Str. 3, A-6020 Innsbruck, Austria

Insulin-like growth factor (IGF) binding protein-3 (IGFBP-3) regulates cell proliferation and survival by extracellular interaction and inactivation of the growth factor IGF-I. Beyond that, IGF-independent actions mediated by intracellular IGFBP-3 including nuclear-IGFBP-3, have also been described. We here show, using both confocal and electron microscopy and cell fractionation, that the extracellular addition of IGFBP-3 to living cells results in rapid uptake and nuclear delivery of IGFBP-3, by yet partly unknown mechanisms. IGFBP-3 is internalized through a dynamin-dependent pathway, traffics through endocytic compartments and is finally delivered into the nucleus. We observed docking of IGFBP-3 containing structures to the nuclear envelope and found IGFBP-3 containing dot-like structures to permeate the nuclear envelope. In summary, our findings establish the pathway by which this tumor suppressor protein is delivered from extracellular space to the nucleus.

Insulin-like growth factors (IGFs) play an important role in regulating cell growth, apoptosis and differentiation in a variety of cell types.[1–3] The activity of both IGF-I and IGF-II is mediated by the IGF type I receptor (IGF-IR). Several secreted IGF binding proteins (IGFBP-1 to 6), serve as transport vehicles for IGFs and control their biological availability.[4] IGFBP-3, a key component of the IGF/IGFBP-axis, plays an important role in tumorigenesis, including breast, prostate and cervical cancer (reviewed in Refs. 4,5). The IGFBP-3 gene is transcriptionally activated by the tumor suppressor p53,[6] and increased expression of IGFBP-3 contributes to both p53-dependent and -independent apoptosis.[6,7] IGFBP-3 was identified as a functional cellular target for the transforming oncoprotein E7 of human papillomavirus 16,[8] and the ability of E7 to induce ubiquitin/proteasome-dependent degradation of IGFBP-3 is required for cell transformation.[8,9] IGFBP-3 also induced apoptosis in human osteosarcoma cells, and apoptosis induction was limited by ubiquitination of IGFBP-3 followed by its proteasomal degradation.[10] Of note, IGFBP-3 was suggested as tumor suppressor in the prostate,[11] and subsequently recombinant IGFBP-3 was shown to induce apoptosis in prostate cancer cells,[7,12] as well as in a transgenic mouse model of prostate cancer.[13]

In addition to IGF-related functions of IGFBP-3, IGF-independent actions of IGFBP-3 contribute to its antiproliferative and proapoptotic activities.[14] Thus, IGFBP-3 can induce programmed cell death in IGF-IR-negative mouse fibroblasts[7]; furthermore, IGFBP-3 mutants that do not bind IGFs can stimulate apoptosis in cancer cells[10,12] and inhibit prostate tumor progression in a transgenic mouse model,[13] suggesting a nuclear function

Key words: IGFBP-3, endocytosis, trafficking, nuclear transport, importin

Abbreviations: GFP: green fluorescent protein; IGF: insulin-like growth factor; IGFBP-3: insulin-like growth factor binding protein-3; LTR: Lysotracker Red DND-99; NLS: nuclear localization signal; siRNA: small interfering RNA; Tf: transferrin

Additional Supporting Information may be found in the online version of this article.

Grant sponsor: Austrian Science Funds; **Grant numbers:** NFN S93, SFB021, P19486-B12, P184468-B12; **Grant sponsor:** European Union INCA project; **Grant number:** LSHC-CT-2005-018704; **Grant sponsor:** BMBWK; **Grant number:** BMBWK-651.048/0001-VI/2/2006); **Grant sponsor:** Austrian National Bank Jubiläumsfonds; **Grant number:** P-11050; **Grant sponsor:** EU (Integrated Project PROTEOMAGE)

Correspondence to: Pidder Jansen-Dürr, Institute for Biomedical Aging Research, Rennweg 10, A-6020 Innsbruck, Austria, Tel.: +43-512-583919-44, Fax: +43-512-583919-8, E-mail: p.jansen-duerr@oeaw.ac.at

of IGFBP-3, probably related to transcriptional regulation. Indeed, IGFBP-3 contains a nuclear localization sequence (NLS) in its conserved C-terminal domain[15] and nuclear localization of IGFBP-3 has been reported in human cancer cells.[16] Accordingly, IGFBP-3 can interact with nuclear transcription factors, such as the retinoid X receptor.[17] Importantly, the extracellular addition of recombinant human IGFBP-3 (rhIGFBP-3) induces cell death in cultured prostate cancer cells (see above), and the infusion of recombinant IGFBP-3 has been successfully used as an experimental therapeutics in a mouse model for prostate cancer.[13] Based on these results, there are attempts to develop therapies for human prostate cancer based on rhIGFBP-3.[18] In view of the potential of rhIGFBP-3 as anticancer drug, it is essential to understand the mechanisms by which extracellular IGFBP-3 acts on tumor cells, and if nuclear functions of IGFBP-3 are relevant for such action. In several cell types, IGFBP-3 can be internalized by endocytosis,[19,20] but the precise mechanisms underlying the cellular uptake of IGFBP-3 are currently not known. In addition, importin-beta-dependent nuclear import of cytosolic IGFBP-3 into the nucleus has been demonstrated in permeabilized Chinese hamster ovary cells,[15] but it is currently unclear whether the same mechanism mediates nuclear uptake of IGFBP-3 in intact cells. We here investigated the dynamics of cellular uptake of IGFBP-3 and its transport to the nucleus by live cell imaging, electron microscopy and biochemical fractionation in human osteosarcoma cells and observed rapid nuclear delivery of IGFBP-3 subsequent to its endocytic uptake.

Material and Methods

Chemicals

All chemicals were purchased from Sigma (Vienna, Austria) unless indicated otherwise.

Cell culture

U-2OS human osteosarcoma cells were obtained from ATCC (American Type Culture Collection, Wesel, Germany) and were maintained in DMEM (Sigma, Vienna, Austria), supplemented with 10% FCS (Biochrom, Berlin, Germany), 2 mM L-glutamine and 100 U/mL penicillin with 0.1 mg/mL streptomycin (Gibco, Invitrogen, Lofer, Austria). The cells were grown in an atmosphere of 5% CO_2 at 37°C and were subcultured by trypsinization with 0.05% trypsin-EDTA (Gibco, Invitrogen, Lofer, Austria) every 3–4 days.

Purification and labeling of human IGFBP-3

Native human IGFBP-3 was produced in U-2OS cells transfected with an IGFBP-3 expression vector, and the protein was isolated from the conditioned supernatant, as described previously.[21] A purification control was performed by subjecting supernatant of mock-transfected U-2OS to the same purification procedure as unlabeled IGFBP-3. IGFBP-3 concentration was determined using a sandwich ELISA (R&D Systems, Abingdon, UK). Purified IGFBP-3 was labeled with AlexaFluor, nanogold and HRP by commercially available kits. A detailed description of labeling procedures is provided in the Supporting Information.

Plasmids and transfection

The mCherry cDNA was kindly provided by Dr. Roger Tsien (Stanford, CA, USA). The mCherry-NLS containing three copies of the SV40 LT NLS was cloned using routine cloning procedures. pEF-NLS-GFP vector was a kind gift from Dr. Stephan Geley (Innsbruck, Austria). pNup153-EGFP plasmid was kindly provided by Dr. Jan Ellenberg (Heidelberg, Germany). Constructs coding for dynamin 2 GFP wild type (WT) and dominant negative K44A[22] were both kindly provided by Dr. Mark McNiven (Rochester, MN, USA). The Rab-7 mCherry construct was kindly provided by Dr. Natalia Schiefermeier (Innsbruck, Austria). U-2OS cells were plated at a density of 5×10^4 cells per well in the 8-well Lab-Tek Chamber Slide System (Nalge Nunc International, Naperville, IL, USA), 6 hr prior to transfection. Cells were transiently transfected with Lipofectamine 2000 (Invitrogen, Lofer, Austria) according the manufacturer's protocol using 0.3 μg of plasmid DNA. On the next day, medium was replaced and experiments were performed within the next 12 hr.

Endocytosis assays and live cell confocal microscopy

For uptake experiments of fluorescence-labeled IGFBP-3, U-2OS cells were plated at a density of 5×10^4 cells per well in the 8-well Lab-Tek Chamber (Nalge Nunc International, Naperville, IL, USA), 24 hr before the experiments were started. Ten μg/mL of AlexaFluor647-labeled IGFBP-3 was added to the cells at the same time as endocytic model substrates. The following concentrations were used: 15 μg/mL Transferrin AlexaFluor568 (Invitrogen, Lofer, Austria), 10 μg/mL Cholera Toxin Subunit B AlexaFluor488 (Molecular Probes, Invitrogen, Lofer, Austria), and 3 mg/mL Dextran AlexaFluor488 (Molecular probes, Invitrogen, Lofer, Austria). For colocalization studies of IGFBP-3 with a marker for acidic vesicles, 75 nM Lysotracker Red DND-99 (LTR; Invitrogen, Lofer, Austria) was used. Cells were coincubated either with IGFBP-3 AlexaFluor647 and LTR for up to 2 hr or preincubated with IGFBP-3 for 2 hr and LTR was added to the cells for additional 5 or 30 min. For nuclear staining, 3 μM Syto16 Green-Fluorescent Nucleic Acid Stain for living cells (Molecular probes, Invitrogen, Lofer, Austria) was used. For 3-D reconstruction of IGFBP-3 nuclear uptake, 10 μg/mL AlexaFluor568- and/or 647-labeled IGFBP-3 was used. Incubation and confocal imaging analysis of U-2OS cells was performed in the 8-well Lab-Tek Chamber (Nalge Nunc International, Naperville, IL, USA). Live cell imaging was performed with a Nipkow disk-based confocal system UltraVIEW RS (Perkin Elmer, Wellesley, MA, USA) and the LSM510META on an Axiovert200 stand equipped with a temperature controlled incubation chamber (Pecon, Erbach, Germany). A detailed description of imaging procedures is provided in the Supporting Information.

Electron microscopy

For uptake experiments of IGFBP-3 conjugated with nanogold or HRP, U-2OS cells were plated at the density of 7.5×10^5 cells per 10 cm culture dish on 3 mm sapphire

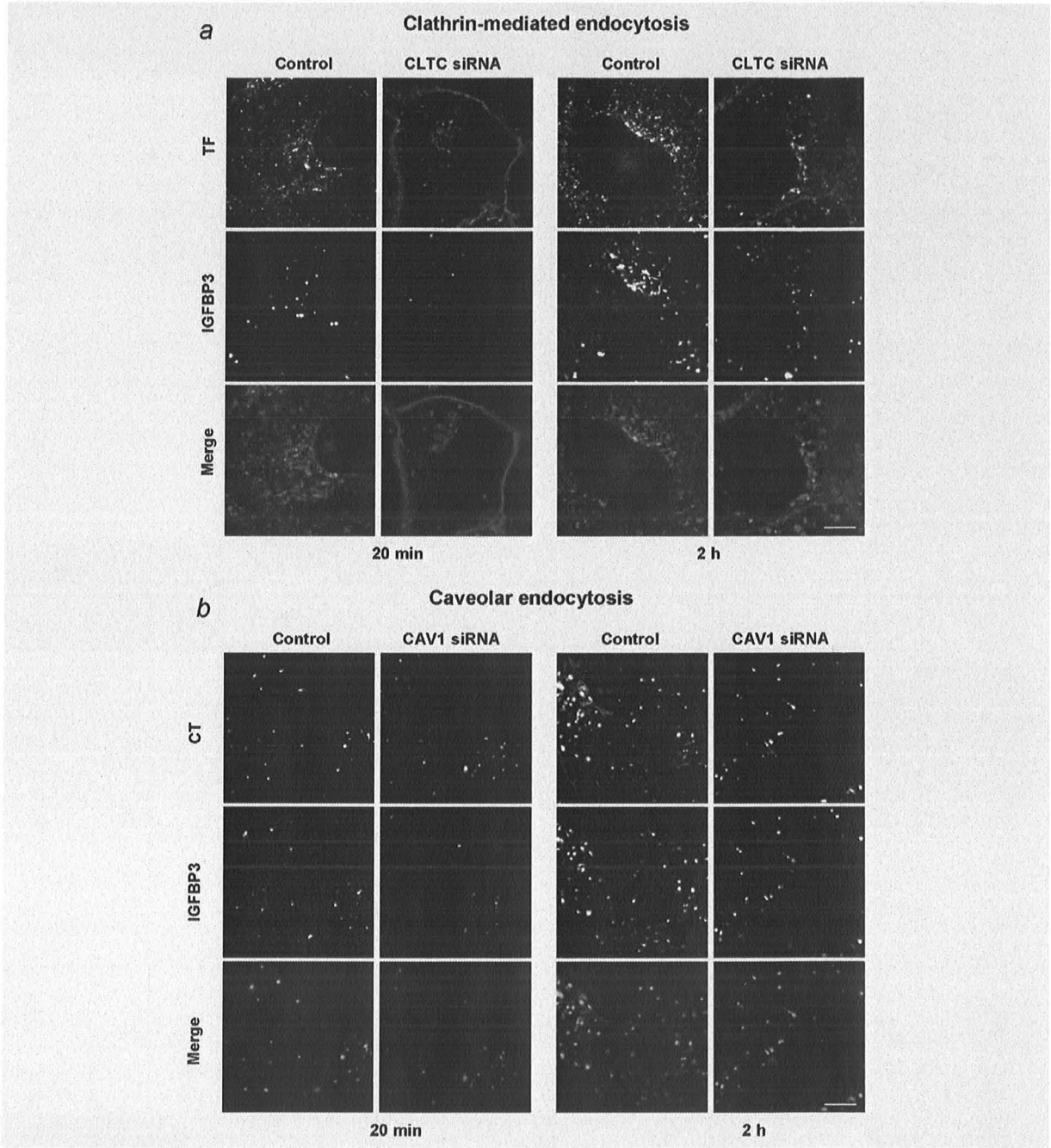

Figure 1. Analysis of IGFBP-3 uptake in U-2OS cells. (*a, b, c*) U-2OS cells were transfected with control siRNAs and siRNAs directed against CLTC, CAV1 and PAK1, as indicated. 24 hr after transfection, cells were monitored 20 min and 2 hr after the addition of AlexaFluor647-labeled IGFBP-3 (red fluorescence) and endocytosis substrates (green fluorescence), as follows: Transferrin AlexaFluor568 (Tf; A), Cholera Toxin Subunit B AlexaFluor488 (CT; B), and Dextran AlexaFluor488 (Dex; C). Representative confocal images are shown. Bar, 5 μm. (*d*) U-2OS cells were co-incubated with Lysotracker Red DND-99 (LTR; red fluorescence) and IGFBP-3 AlexaFluor647 (green fluorescence) added at the same time. Confocal images were taken after 20 min and 2 hr, as indicated. Representative pictures are shown. Bar, 2 μm. (*e*) Upper plot represents the relative percentage of labeled vesicles staining positive for IGFBP-3, each of the reference markers (Tf, CT, Dex, LTR) and/or both. Lower plot shows the percentage of IGFBP-3 positive vesicles colocalizing with each of the reference markers. The results of two representative experiments are shown. Bars represent the mean value of 16 independent cells ± SEM. (*f*) Analysis of IGFBP-3 uptake in U-2OS cells after inhibition of the three major endocytic pathways using siRNA for clathrin heavy chain (CLTC), caveolin 1 (CAV1) and/or p21 protein (Cdc42/Rac)-activated kinase 1 (PAK1). As a control, scrambled siRNA (SCR) was used. Upper plot shows the percentage of IGFBP-3 positive vesicles 20 min and 2 hr after the addition of IGFBP-3 to the cells transfected with the specific siRNAs as indicated. To verify the efficiency of individual siRNAs, uptake of markers for each endocytic pathways (Tf, CT, Dex) was monitored in knock down cells as indicated (Lower plot). The results of two representative experiments are shown. Bars represent the mean value of 16 independent cells ± SEM. The efficiency of knock down was also confirmed by Western blot, 72 hr after the transfection. [Color figure can be viewed in the online issue, which is available at wileyonlinelibrary.com.]

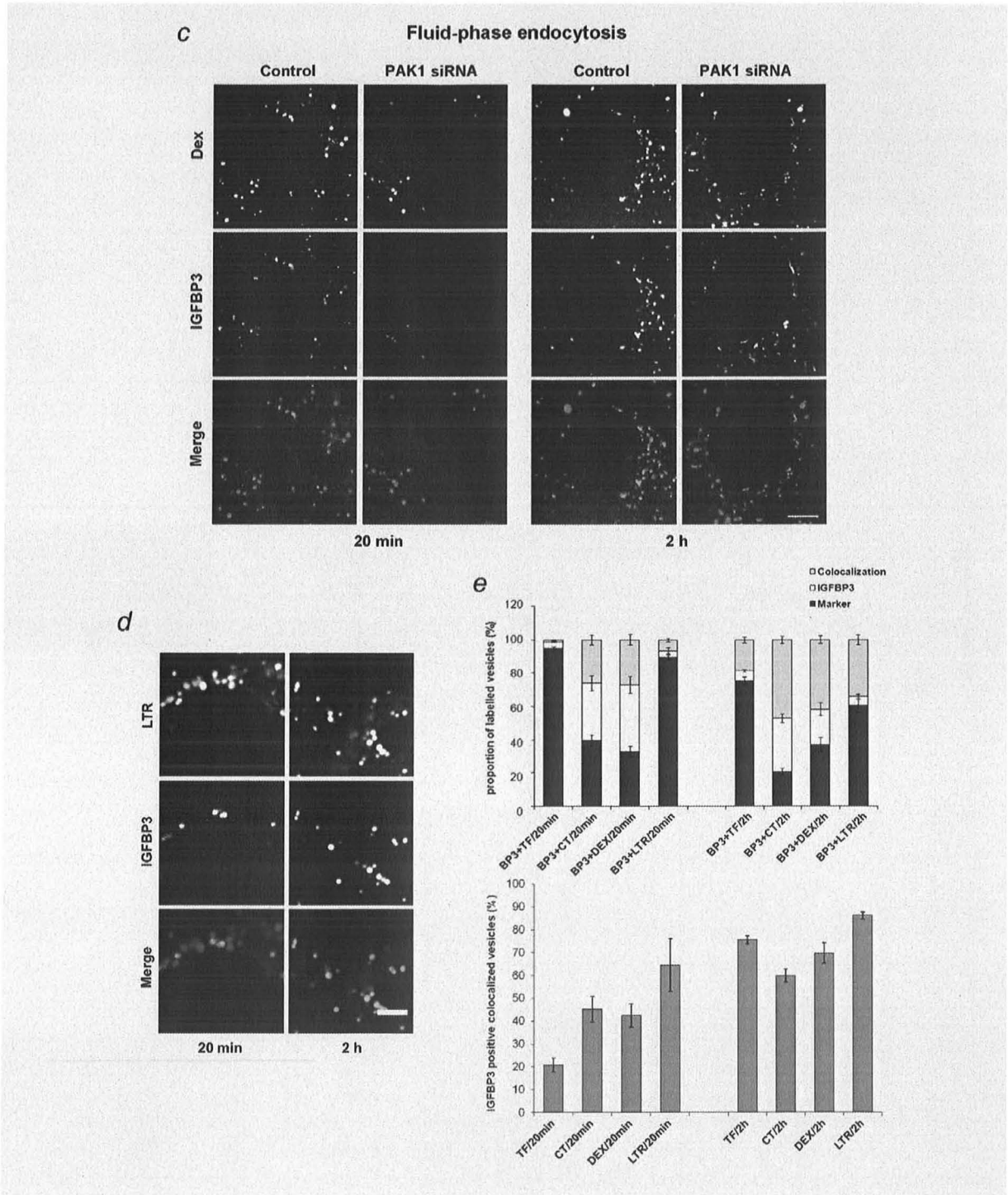

Figure 1. (Continued)

coverslips.[23] Uptake was initiated by the addition of 10 μg/mL nanogold or HRP labeled IGFBP-3 to the medium. As a negative control, nonconjugated nanogold (Nanoprobes, Yaphank, NY, USA) or HRP (Sigma, Vienna, Austria) was used. After 2–4 hr incubation, cells were processed for electron microscopy. Conventional chemical fixation (2.5% v/v

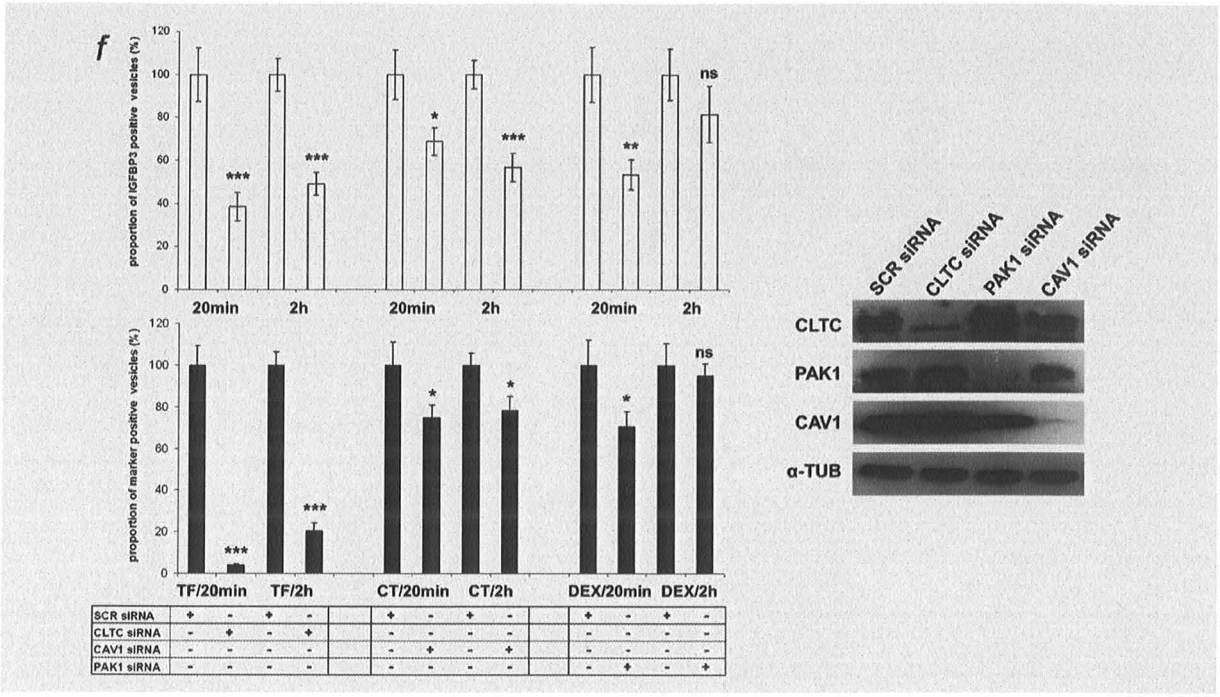

Figure 1. (Continued)

glutaraldehyde in 0.1 M phosphate buffer, pH 7.4, 120 min, RT) yielded unsatisfactory preservation of cytoplasmic organelles in preliminary experiments. Therefore, cryo-based specimen fixation (high-pressure freezing) was employed. Subsequently, samples were subjected to freeze-substitution (with acetone containing 0.5% (v/v) glutaraldehyde, optionally supplemented with 0.2% (w/v) uranyl acetate and 4% (v/v) water) and sample rehydration.[24,25] Samples were rinsed with double distilled water and subjected to silver enhancement—when appropriate—(HQ-Silver (Nanoprobes, Yaphank, NY, USA), 7–9 min, RT) of the 1.4 nm-small nanogold particles.[26] This enhancement procedure produced in our case particles of ~35 nm with almost no unspecific background. IGFBP-3-HRP was visualized by means of DAB-cytochemistry.[24] After short postfixation with aqueous OsO_4 (1% w/v), samples were embedded in epoxy resin and serial thin sections were viewed with a Philips CM120 transmission electron microscope that was equipped with a goniometer stage.

Cell fractionation and immunoblotting

For uptake of unlabeled IGFBP-3 protein, U-2OS cells were seeded in a culture dish to reach a density of 80% at the day of the experiment. Cells were incubated with 15 μg of rhIGFBP-3 in serum-free DMEM for 2 hr. Supernatants from mock-transfected U-2OS cells, purified in the same way as IGFBP-3 supernatants, were used as control. For fractionation experiments, U-2OS cells were cultured in 75 cm^2 flasks. The cells were harvested in 0.05% trypsin-EDTA (Gibco, Invitrogen, Lofer, Austria). Cells were washed four-times with cold PBS and fractionated into three different cellular compartments (cytosol, membranes and nucleus) by Qproteome Cell Compartment Kit (Qiagen, Vienna, Austria), according the manufacturer's instructions. Purity of individual fractions was verified by Western blot analysis using antibodies against specific markers for each fraction, as described.[10] The following antibodies were used for Western blot analysis: goat polyclonal antibody to IGFBP-3 (R&D Systems, Abingdon, UK); mouse monoclonal antibody to nuclear matrix protein p84 (Abcam, Cambridge, UK); mouse monoclonal antibody to ATP-synthase subunit alpha (ATP5A1; Molecular probes, Invitrogen, Lofer, Austria); goat antipyruvate kinase (rabbit muscle) antibody (M2PK; Rockland, Gilbertsville, PA, USA). For a quantitative assessment of IGFBP-3 uptake, IGFBP-3 protein gels were run exceptionally short-time to allow all IGFBP-3 isoforms to be quantified as a single band.

Results

To evaluate the biological activity of recombinant native IGFBP-3, the protein was added to U-2OS osteosarcoma cells, which were then monitored over a total of 2 cell cycles (*ca.*, 32 hr). Under these conditions, we observed a moderate but significant increase in the number of apoptotic cells

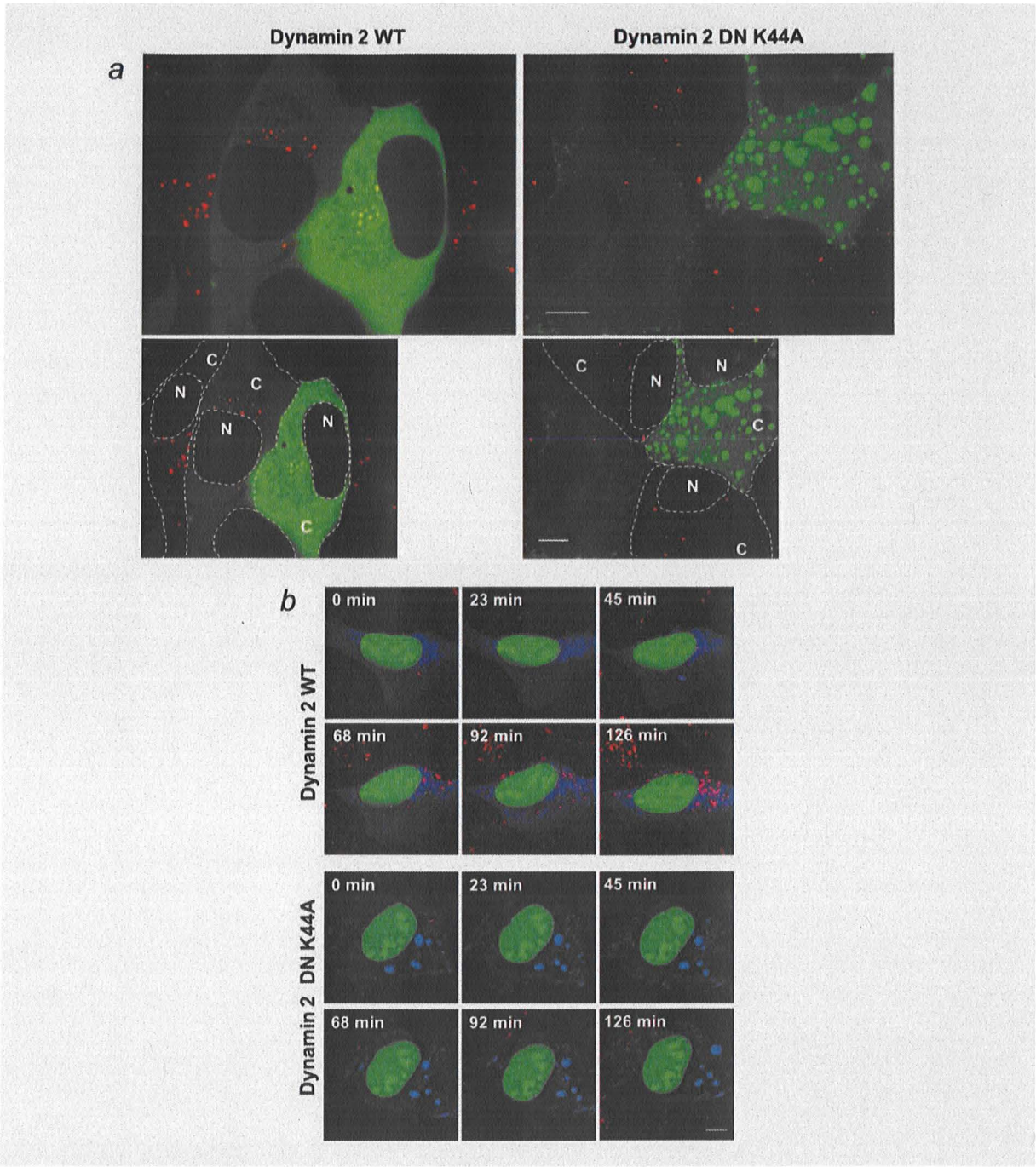

Figure 2. IGFBP-3 uptake requires dynamin 2. (*a*) U-2OS cells were transfected with expression vectors coding for GFP fusion proteins containing dynamin 2 WT or dominant negative (DN) K44A, as indicated (green fluorescence). 24 hr after transfection, IGFBP-3 AlexaFluor647 (red fluorescence) was added and cells were analyzed by confocal live cell microscopy after 30 min. Representative pictures are shown. Bar, 5 μm. In the lower panels, contours of both transfected and untransfected cells were drawn for their better visualization. (*b*) Cells were co-transfected with expression vectors coding dynamin 2 GFP WT or DN K44A (blue fluorescence) and for nuclear fluorescent protein mCherry (here: green fluorescence), as indicated. 24 hr after transfection, IGFBP-3 AlexaFluor647 (red fluorescence) was added and cells were monitored by confocal live cell microscopy for 2 hr. mCherry nuclear fluorescence was used as a marker for the autofocus and tracking macro. Images of two representative cells obtained at the indicated time points are shown. Bar, 10 μm.

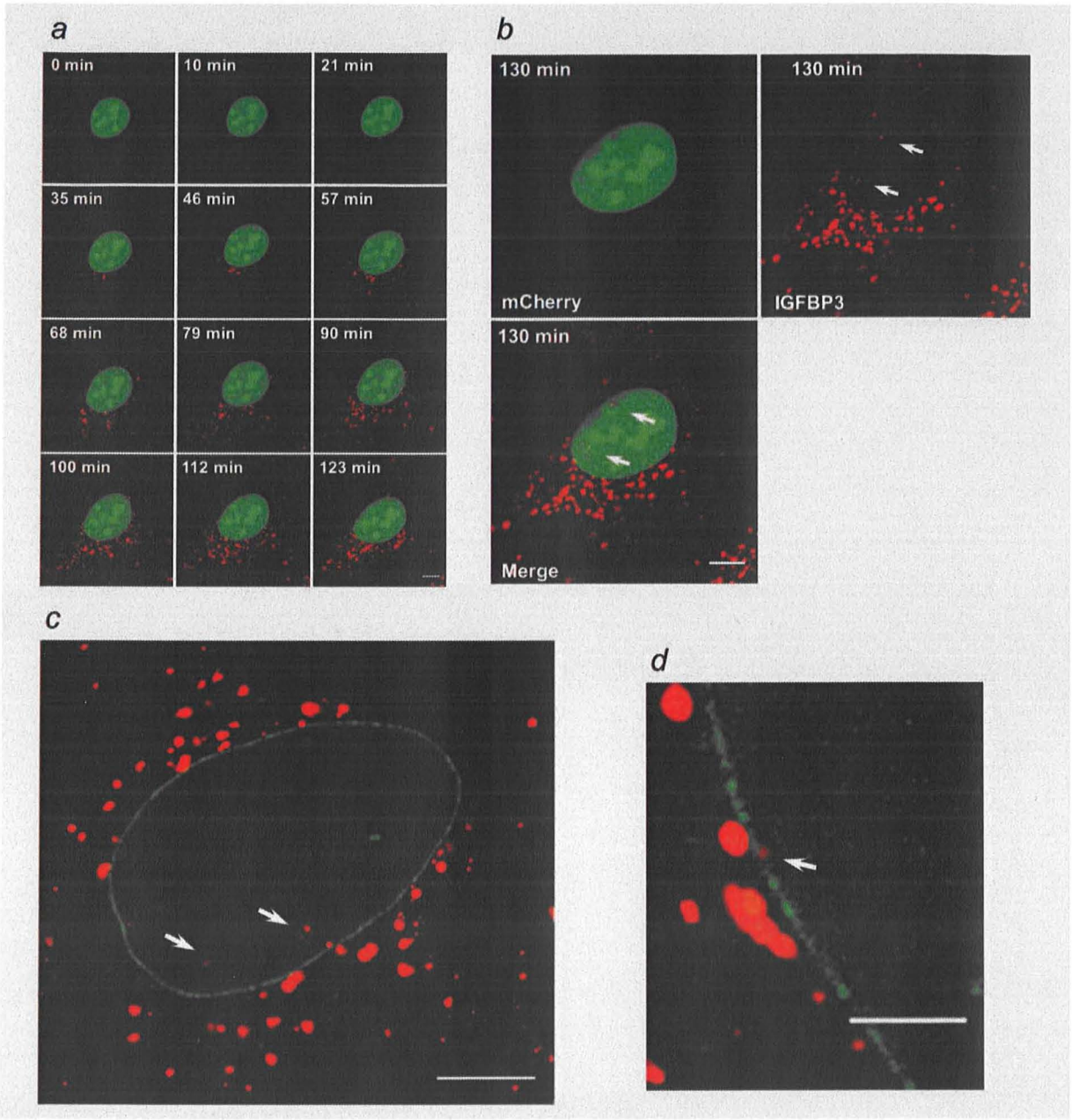

Figure 3. Kinetics of IGFBP-3 uptake and nuclear delivery. (*a*) U-2OS cells were transfected with expression vector coding for nuclear fluorescent protein mCherry (here: green fluorescence). Twenty-four hours after transfection, IGFBP-3 AlexaFluor647 (red fluorescence) was added, and eight individual cells were analyzed by confocal live cell microscopy at the indicated time points. mCherry nuclear fluorescence was used as a marker for the autofocus and tracking macro. Confocal images of one representative cell monitored over 2 hr are shown. Bar, 10 μm. (*b*) U-2OS cells were treated as in panel *a*. Accumulation of IGFBP-3 in the cytoplasm and nucleus of U-2OS cells is shown at 130 min after IGFBP-3 addition. Arrows indicate IGFBP-3 containing dot-like structures in the nucleus. Bar, 10 μm. (*c*) U-2OS cells were transfected with expression vector for Nup153-GFP (green fluorescence). Twenty-four hours after transfection, AlexaFluor647-labeled IGFBP-3 (red fluorescence) was added, and cells were analyzed by confocal live cell microscopy. One representative image is shown. Arrows point to IGFBP-3 containing dot-like structures in the nucleus. Bar, 5 μm. (*d*) U-2OS cells were treated as in panel C and analyzed by time-resolved confocal live cell microscopy. Bar, 2 μm. Shown here is an enlarged image of a region of interest which was used to record in a videoclip the delivery of IGFBP-3 to the nucleus (movie provided as Supporting Information, Video3D.mov).

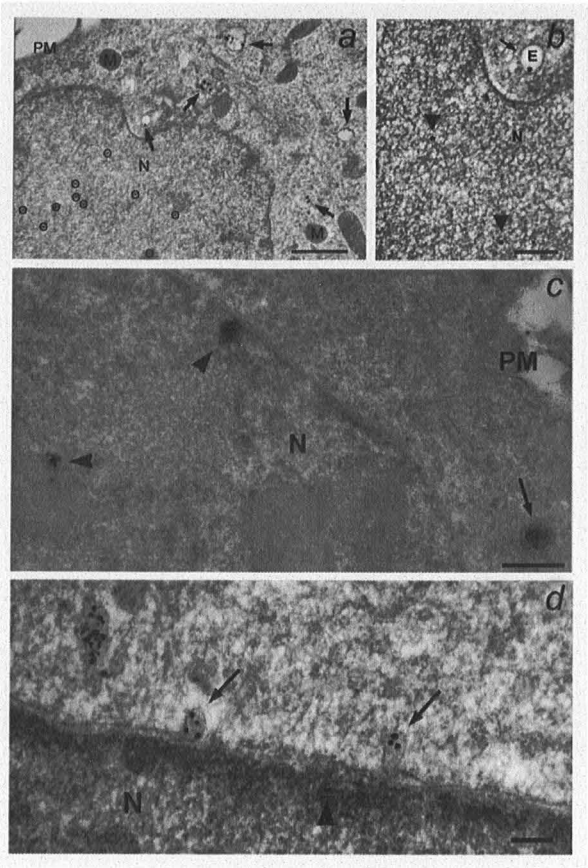

Figure 4. Electron microscopy of U-2OS cells incubated with IGFBP-3-nanogold (panels *a*, *b*, *d*) or with IGFBP-3-HRP (panel *c*). Panel *a* shows IGFBP-3-nanogold-silver particles inside endocytic compartments (arrows) and within the nucleus (N) after 2 hr of incubation; singular nuclear gold-silver particles are encircled for better visibility; PM = plasma membrane, M = mitochondrion. Bar, 1 μm. Panel *b*: detail of panel *a*. Cytoplasmic IGFBP-3-nanogold-silver locating inside an endosome (E: arrow) *versus* nuclear IGFBP-3-nanogold-silver lying freely within the nucleus (arrow heads). Bar, 200 nm. In panel *c*, IGFBP-3-HRP (arrow-heads) is seen after 4 hr of incubation within the nucleus (N) and inside an endosome (arrow); PM = plasma membrane. Bar, 500nm. Panel *d* shows endosomal vesicles containing IGFBP-3-nanogold-silver particles (arrows) in intimate contact with the nuclear envelope (a singular gold particle inside the nucleus (N) is marked by an arrow-head). Bar, 200 nm.

(Supporting Information Fig. S1) along with a reduced number of mitotic cells (Supporting Information Fig. S1), consistent with previous studies,[4,10] suggesting that U-2OS cells are a suitable model system to study IGFBP-3 uptake. Subsequently, recombinant native IGFBP-3 was labeled with two distinct fluorescent dyes, AlexaFluor568 and 647, and used for live cell imaging. IGFBP-3 was efficiently labeled with both dyes (Supporting Information Fig. S2) and retained biological functions, *e.g.*, to sequester IGF-I and thereby suppress AKT signaling[27] (Supporting Information Fig. S3). U-2OS cells were then coincubated with fluorescent IGFBP-3 and fluorescent model cargoes for clathrin-mediated endocytosis, caveolar endocytosis and fluid-phase endocytosis, respectively.

When IGFBP-3 was added along with transferrin (Tf), Tf-positive vesicular structures were readily observed after 20 min, whereas the uptake of IGFBP-3 was much slower. We found that at early time points the vast majority of Tf-positive vesicles were negative for IGFBP-3, and only a minor proportion of IGFBP-3 containing vesicles were also positive for Tf (Fig. 1*a*). Two hours after the addition of both substrates, 19 ± 1.9% of all detected vesicles were both IGFBP-3 and Tf positive (Figs. 1*a* and 1*e*). Although it was suggested that IGFBP-3 is internalized in a complex with Tf,[28] our observation, that the uptake of both proteins follows a largely different kinetics (Tf uptake being much faster) would argue against joint uptake of both proteins in a specific complex. Shortly after coaddition of cholera toxin (CT) and IGFBP-3 to study caveolar endocytosis, codistribution of both proteins was observed in 26 ± 3.0% of the vesicles (20 min). After 2 hr, 47 ± 2.2% of the vesicles were positive for both IGFBP-3 and CT (Figs. 1*b* and 1*e*). When fluorescent dextran (Dex; Figs. 1*c* and 1*e*), a marker for fluid-phase endocytosis and IGFBP-3 were coadministrated, 27 ± 3.1% were colocalized after 20 min and 42 ± 2.3% after 2 hr.

Whereas in each experiment only those vesicles were visible (and therefore counted) that were positive for either IGFBP-3, the control cargo, or both, the density of IGFBP-3 positive vesicles per cell was similar in all uptake experiments (Supporting Information Fig. S4). These data indicate that all three uptake routes studied here contribute to the net uptake of IGFBP-3. This point was further addressed by RNA interference targeting specific components of endocytic pathways, *i.e.*, clathrin heavy chain[29] for the clathrin coated pit pathway, caveolin 1[30] for caveolar endocytosis and PAK1 for fluid-phase endocytosis.[31] We found that knocking down either clathrin heavy chain or caveolin 1, both reduced the internalization of IGFBP-3, suggesting that IGFBP-3 uptake indeed utilizes both clathrin-mediated and caveolin-mediated endocytosis (Figs. 1*a*, 1*b*, and 1*f*). After knocking down PAK1, IGFBP-3 uptake was reduced at an early time point (20 min), whereas at later time points the effect was no longer visible. These findings suggest that fluid-phase endocytosis mainly contributes to early steps of IGFBP-3 uptake (Figs. 1*c* and 1*f*).

To address the relationship between IGFBP-3 containing vesicles and endosomes/lysosomes, acidic vesicles (*i.e.*, mainly lysosomes) were labeled with Lysotracker Red DND-99 (LTR). Twenty minutes after the addition of IGFBP-3 and LTR, 65 ± 11% of IGFBP-3 containing vesicles also contained LTR and this ratio increased to 86 ± 1.6% after 2 hr (Figs. 1*d* and 1*e*). The number of LTR positive vesicles containing also IGFBP-3, increased from 6% (20 min) to 36% (2 hr). The predominant presence of intracellular IGFBP-3 in endosomes/lysosomes was confirmed in a second set of

experiments, where LTR was added to the cells 2 hr after adding IGFBP-3. Shortly after addition of LTR, nearly all IGFBP-3 containing vesicles showed LTR fluorescence (Figure S5). The data suggest that IGFBP-3 is mainly contained in endosomes/lysosomes after internalization.

Most if not all endocytic processes depend on dynamin, which is required for vesicle movements.[32] To address the role of dynamin in IGFBP-3 uptake, we expressed GFP fusion proteins either of WT dynamin 2 or its dominant negative mutant (K44A), which is unable to support endocytic

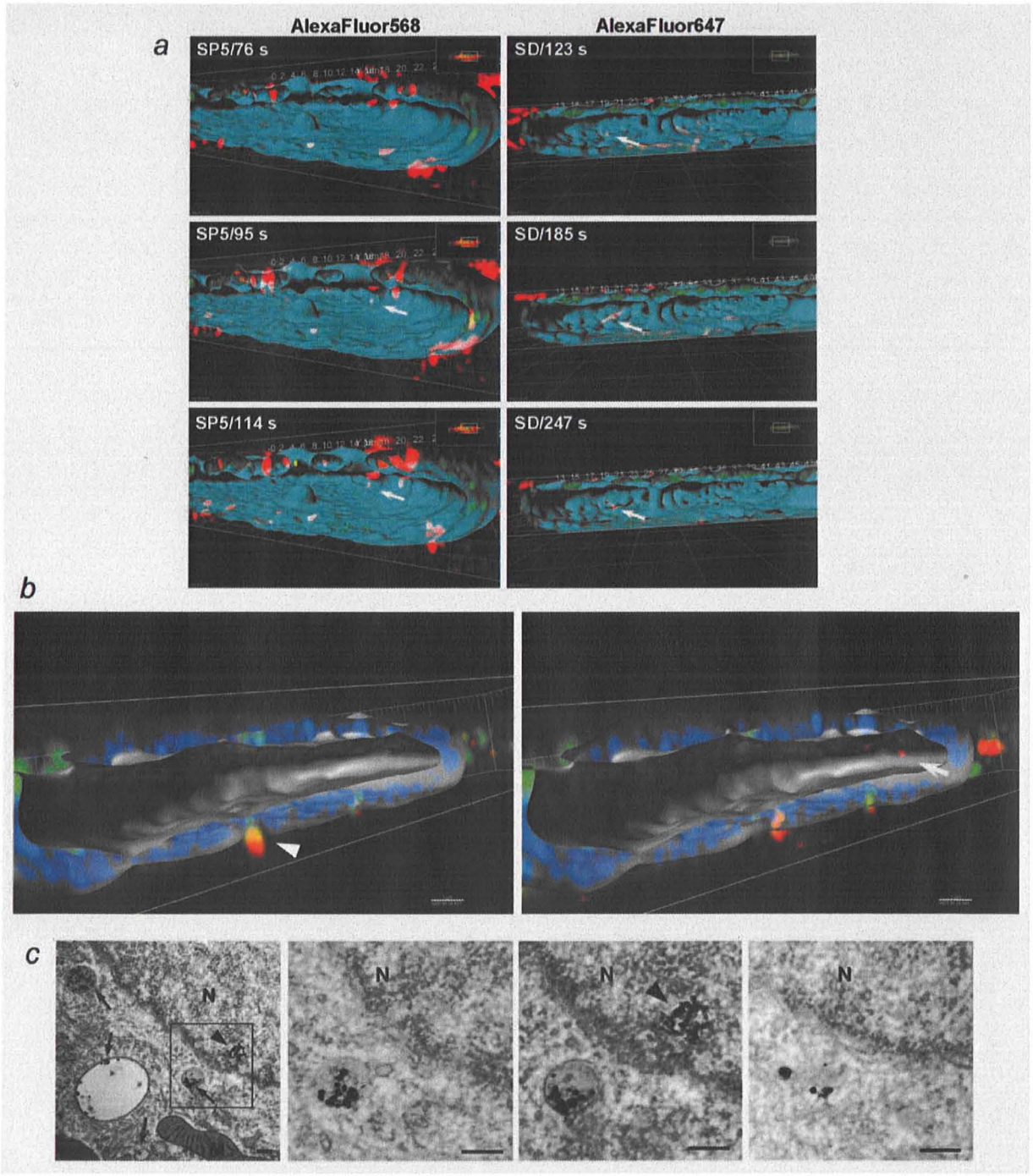

Figure 5.

uptake of extracellular substrates.[22] In both experiments, untransfected (GFP negative) cells served as internal controls. IGFBP-3 was added to transfected cells and its uptake was studied by live cell imaging. Within 30 min, cells expressing WT dynamin 2 readily internalized IGFBP-3, in contrast to cells expressing the K44A mutant (Fig. 2*a*). We, furthermore, monitored uptake of IGFBP-3 for 2 hr by confocal microscopy. We observed time-dependent accumulation of IGFBP-3 in cells overexpressing WT dynamin 2, whereas this process was impaired in cells expressing dominant negative dynamin 2 (Fig. 2*b*, Supporting Information Fig. S6), confirming that dynamin 2 function is essential for uptake of extracellular IGFBP-3.

To study nuclear uptake of IGFBP-3, its subcellular localization was monitored by time lapse confocal microscopy over 2 hr using U-2OS cells expressing NLSmCherry.[33] With increasing incubation time, we observed the accumulation of IGFBP-3 containing vesicles in the cytoplasm. At later time points, IGFBP-3 containing vesicles were found in close association with the nucleus (Fig. 3*a*), and rarely, a few discrete IGFBP-3 containing dot-like structures were detected inside the nucleus (Fig. 3*b*), along with an increase in overall IGFBP-3 nuclear staining (Supporting Information Fig. S7). A similar increase in nuclear IGFBP-3 was observed in cells expressing WT dynamin 2 but not in cells expressing the mutant K44A (Supporting Information Fig. S8).

To define the outline of the cell nucleus, nucleoporin 153-GFP fusion protein (Nup153-GFP),[34] was expressed in U-2OS cells before fluorescent IGFBP-3 was added. After 2 hr, IGFBP-3 was clearly present within the nucleus (Fig. 3*c*) and dynamic interaction of IGFBP-3 containing vesicles with the nuclear envelope and the eventual transfer of IGFBP-3 containing dot-like structures into the nucleoplasm (Fig. 3*d*, Supporting Information, Video3D.mov) was observed. Nuclear delivery of IGFBP-3 was also analyzed using the nuclear counterstain Syto16, added a few seconds before time lapse confocal microscopy was started (Fig. S9). In this experiment, we observed fast translocation of IGFBP-3 into the nucleus (Supporting Information, VideoS9.mov). The rapid disappearance of nuclear IGFBP-3 containing structures observed here may be due to rapid diffusion; it may be further enhanced by the fact that nuclear IGFBP-3 is subject to ubiquitin/proteasome-dependent proteolysis.[10]

To study the uptake and intracellular distribution of extracellularly administrated IGFBP-3 by cryo-based electron microscopy, IGFBP-3 was covalently linked to nanogold particles or HRP (Fig. S2). Two to 4 hr after addition to the cells, IGFBP-3 labeled by either method was localized both within endocytic vesicles and inside the nucleus of morphologically intact cells (Figs. 4*a*, 4*b*, and 4*c*). As in fluorescence microscopy, IGFBP-3 containing vesicles were found in close contact with the nuclear envelope (Fig. 4*d*). Unconjugated nanogold particles or HRP were used as controls, which yielded virtually no intracellular nanogold particles or intranuclear HRP-DAB-reaction product, respectively (data not shown).

To further explore nuclear delivery of exogenously added IGFBP-3, we acquired high resolution 4D reconstructions using confocal live cell microscopy followed by deconvolution. The obtained images confirmed the presence of IGFBP-3 containing dot-like structures in the nucleus several hours after addition of IGFBP-3 to the cells (Supporting Information Fig. S10; see Supporting Information Fig. S11 for raw data without deconvolution). The restored images clearly revealed highly dynamic intranuclear IGFBP-3 containing structures (Fig. 5*a*; see Figure S12 for the exact cutting position). To further address the pathway underlying IGFBP-3 nuclear import, we used mCherry-tagged Rab-7 as a specific marker for late endosomes (Fig. 5*b*). These experiments confirmed that IGFBP-3 is present in late endosomes only prior to nuclear uptake and demonstrated that IGFBP-3 in the nucleus was not associated with Rab-7.

A 3D analysis of ultrastructural data was also performed. Using EM serial sections, we found IGFBP-3-nanogold clusters in the nucleus which were entirely located in the

Figure 5. Time resolved 3D reconstruction of IGFBP-3 nuclear uptake. (*a*) Time course 3D reconstructions. U-2OS cells were transfected with Nup153-GFP (green fluorescence) and incubated for 3 hr with IGFBP-3 (red fluorescence) labeled by either AlexaFluor568 or AlexaFluor647 as indicated. Data were recorded by confocal laser scanning microscopy (SP5, left panel) and confocal spinning disc microscopy (SD, right panel). 3D stacks were acquired continuously over time, deconvolved and processed by Imaris software as described in Material and Methods. 3D reconstructions were made of Nup153 and IGFBP-3 positive structures, showing the nuclear interior (perspective scale; grid major tick, 2 μm). The isosurface rendered to Nup153-GFP, corresponding to the inner and outer borders of the nuclear envelope, is shown in cyan. Note the isolated red IGFBP-3 containing structures in the nucleus indicated by arrows (see Supporting Information Fig. S10 for orthogonal sections after deconvolution, S11 for raw data without deconvolution and Supporting Information Fig. S12 for the exact cutting positions). (*b*) 3D reconstructions of U-2OS cells transfected with Nup153-GFP (blue fluorescence), Rab-7 mCherry (green fluorescence) 3 hr after the incubation with IGFBP-3 AlexaFluor647 (red fluorescence) are shown (nuclear interior: perspective scale; grid major tick, 2 μm). The isosurface rendered to Nup153, corresponding to the inner and outer borders of the nuclear envelope, is shown in grey. Note the isolated red IGFBP-3 containing structures in the nucleus (arrow), and IGFBP-3 colocalized with Rab-7 in the cytoplasm and in close contact with the nucleus (arrow head). (*c*) Three-dimensional EM-analysis of the nuclear localization of exogenously added IGFBP-3: A series of consecutive 100 nm-thin sections through the area framed in the overview clearly revealed a cluster of nuclear IGFBP-3-nanogold (arrowhead) without any connection to the surrounding cytoplasm; M = mitochondrion, N = nucleus; arrows mark endosomes/lysosomes containing IGFBP-3-nanogold. Bar, 200 nm.

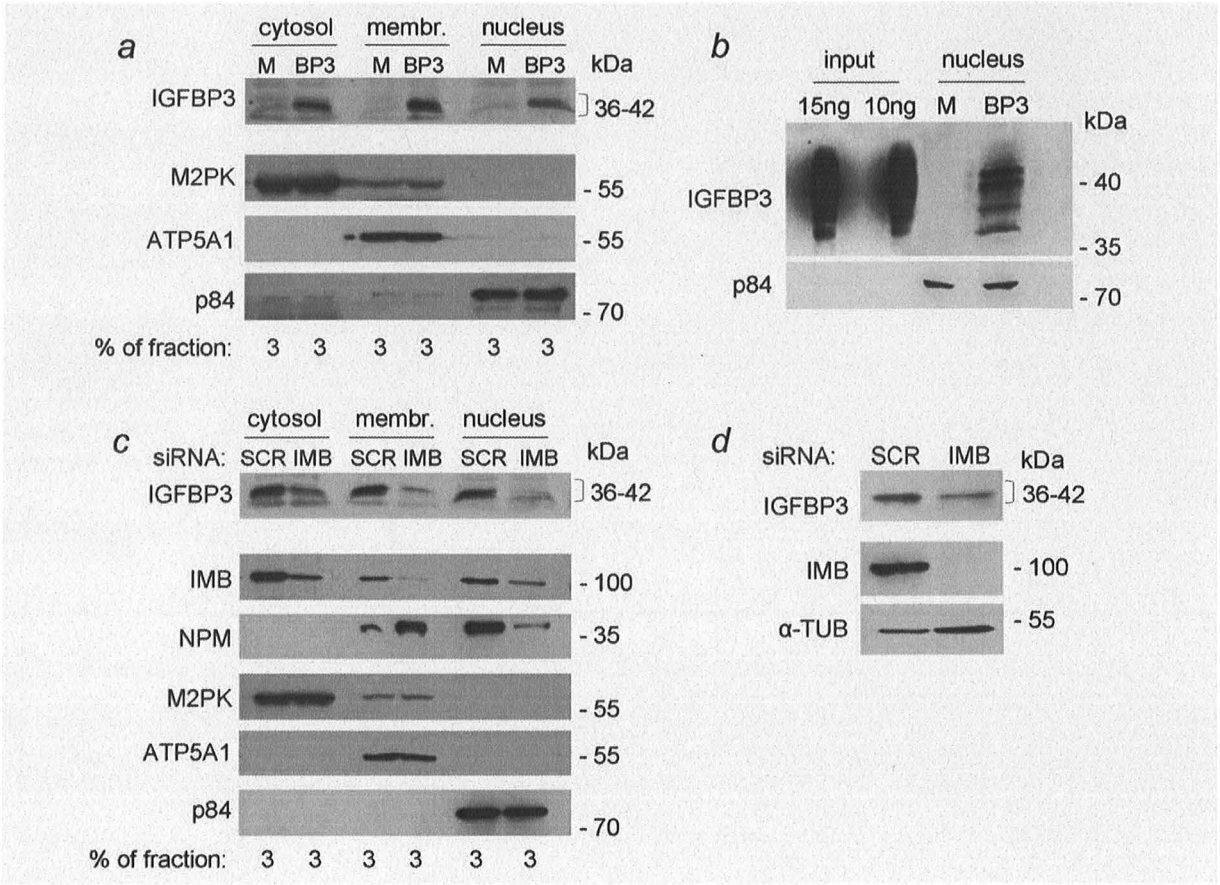

Figure 6. Nuclear delivery of endocytosed IGFBP-3 requires importin-beta. (*a*) U-2OS cells were incubated with unlabeled IGFBP-3 (BP3) or purification control from mock-transfected cells (M) for 2 hr. Subsequently, cells were harvested and fractionated into cytosolic, membrane, and nuclear fraction, as indicated. Equal aliquots (3%) of each fraction were loaded on SDS-PAGE for comparison. The distribution of IGFBP-3 protein in individual compartments was analyzed by Western blot. Purity of subcellular fractions was verified by Western blot using specific markers for each compartment. Nuclear fraction: nuclear matrix protein p84 (p84); cytosolic fraction: pyruvate kinase M2 (M2PK); membrane fraction: ATP synthase subunit alpha (ATP5A1). Please note that for IGFBP-3 quantification, IGFBP-3 gels were run exceptionally short-time and the IGFBP-3 isoforms appear as a single band. (*b*) Quality of IGFBP-3 protein was tested by Western blot. 10 and 15 ng of purified IGFBP-3 protein used for uptake experiments (input), along with IGFBP-3 retrieved from nuclear fraction were separated on SDS-PAGE as indicated. For optimal comparison of the IGFBP-3 isoforms, the gel was run under standard conditions. Purity of nuclear fraction was verified as described in panel *a*. (*c*) U-2OS cells were transfected with siRNA specific for importin-beta (IMB) and scrambled siRNA (SCR), as indicated. Seventy-two hours after transfection, unlabeled IGFBP-3 was added to the cells followed by incubation for 2 hr. Cells were fractionated and analyzed as in panel A. Equal aliquots (3%) of each fraction were loaded on SDS-PAGE for comparison. Levels of IGFBP-3, importin-beta and nucleophosmin (NPM) were analyzed by Western blot. Purity of individual fractions was verified by Western blot using specific markers for each compartment, as described for panel A. Please note that for IGFBP-3 quantification, IGFBP-3 gels were run exceptionally short-time and the IGFBP-3 isoforms appear as a single band. (*d*) Levels of IGFBP-3 and importin-beta (IMB) in total cell lysates of U-2OS cells transfected with either scrambled (SCR) or importin-beta siRNA were analyzed as described in panel *c*. As a loading control, α-tubulin (α-TUB) was used. Please note that for IGFBP-3 quantification, IGFBP-3 gels were run exceptionally short-time and the IGFBP-3 isoforms appear as a single band.

nucleoplasm with no connection to the cytoplasm (Fig. 5*c*), clearly showing that extracellular IGFBP-3 was delivered into the nucleus.

To further explore the nuclear uptake of IGFBP-3 from the extracellular space using a biochemical assay, unlabeled IGFBP-3 was added to U-2OS cells, which contain low levels of endogenous IGFBP-3,[10] followed by cell fractionation. To determine the distribution of IGFBP-3 between different cellular subfractions, equal aliquots of each fraction (3%) were loaded on SDS-PAGE and analyzed by Western blot using

IGFBP-3 antibodies. Two hours after addition to U-2OS cells, IGFBP-3 was detected in the nuclear fraction by Western blot (Fig. 6*a*). This observation may reflect IGFBP-3-containing vesicles that are tightly associated with the nucleus and/or IGFBP-3 molecules inside the nucleus. All major IGFBP-3 bands could be retrieved from the nuclear fraction, when compared with the input IGFBP-3 preparation (Fig. 6*b*). Apparently, intact IGFBP-3 reaches the nuclear fraction, suggesting that if IGFBP-3 is degraded in the acidic vesicles, this process is quite inefficient.

Because importin-beta is the main import factor required for nuclear import of cargo from the cytosol,[35] we addressed its role in nuclear import of IGFBP-3. When importin-beta was depleted by specific siRNA (Fig. 6*c*), we observed a reduction of nuclear nucleophosmin, a well-known cargo of the importin-dependent nuclear import pathway.[36] Depletion of importin-beta also led to a significant reduction in the abundance of nuclear IGFBP-3 to 29 ± 9.5% (Fig. 6*c*). This observation suggests that the classical nuclear import pathway contributes at least partially to nuclear uptake of internalized IGFBP-3. However, the general rate of IGFBP-3 uptake was also reduced in U-2OS cells, upon importin-beta depletion (Fig. 6*d*), rendering further conclusions about the role of importin-beta in the nuclear import of IGFBP-3 rather difficult.

Discussion

We here provide detailed information about the uptake route of rhIGFBP-3 in living human cancer cells. The key observation described in this report is that the addition of recombinant human IGFBP-3 to living human osteosarcoma cells results in the rapid (2 hr) appearance of IGFBP-3 in the nucleus. This finding is backed up by time lapse confocal microscopy of IGFBP-3 endocytosis, by electron microscopy, and by cell fractionation experiments.

IGFBP-3 endocytosis

Endocytic uptake of IGF binding proteins, such as IGFBP-3[19,20] and IGFBP-5[19,37] was described before. Concerning IGFBP-5, the mechanisms of cellular and nuclear delivery have been discussed controversially,[38] and one recent study came to the conclusion that nuclear uptake of extracellular IGFBP-5 does not occur in intact cells but requires the prior permeabilization of the cellular membranes.[37] In our study, we demonstrate nuclear uptake of extracellular IGFBP-3 in intact living cells, and our results provide new information on this process. As the model substrates Tf, CT and Dex all partly colocalized with IGFBP-3 during endocytosis, we conclude that IGFBP-3 uses the three major endocytic pathways, *i.e.*, the caveolin dependent endocytic route, the clathrin coated pit endocytic pathway and the fluid-phase endocytic pathway.

Further evidence supporting multiple uptake mechanisms came from experiments with siRNA-mediated gene silencing. Thus, knock down of caveolin 1 and clathrin heavy chain significantly reduced the number of IGFBP-3 containing vesicles. Consistent with a major involvement of endocytic pathways for IGFBP-3 uptake, dynamin 2, a common hub of the main endocytic pathways[39] was absolutely required for uptake of IGFBP-3. Whereas TGF-beta receptor type V was described as a cell surface receptor for IGFBP-3,[40] the membrane receptor(s) of IGFBP-3 required for the clathrin coated pit endocytic pathway remain to be identified. Whereas in principle receptor-independent fluid phase uptake could be sufficient for IGFBP-3 delivery across the plasma membrane, our data do not suggest a major role for fluid-phase endocytosis for IGFBP-3 uptake.

Nuclear localization of IGFBP-3

Based on immunofluorescence studies with fixed cells, others reported quite uniform nuclear localization of IGFBP-3 in IGFBP-3 secreting PC-3 prostate cancer cells.[20] In our study, we detected IGFBP-3 clusters as well as homogenously distributed IGFBP-3 throughout the nucleus both by LM and EM. Whereas we used one and the same recombinant IGFBP-3 for the different assays, the protein had to be differently labeled for each particular imaging application. However, we believe that the observed patterns reflect a genuine biological phenomenon and are not merely a consequence of using different labels, because distinct as well as diffuse intranuclear IGFBP-3 signals were independently observed by various LM and EM techniques. Thus, nuclear IGFBP-3 forms quite large, short-lived objects, which are devoid of the late endosomal marker Rab-7. One possible explanation for the observed bimodal distribution of nuclear IGFBP-3 is rapid diffusion of transient IGFBP-3 clusters after their entry into the nucleus.

Because experiments with permeabilized cells suggested importin-dependent nuclear import of IGFBP-3,[15] we explored the role of importin-beta in IGFBP-3 trafficking. Indeed, the depletion of importin-beta reduced the levels of nuclear IGFBP-3 (Fig. 6*c*), indicating that the importin pathway contributes to nuclear delivery of IGFBP-3. However, importin-beta knock down also significantly reduced the total uptake of IGBFP-3 (Fig. 6*d*), suggesting that the observed loss in nuclear localisation may partly be due to a general reduction of IGFBP-3 endocytosis. Generally, the underlying mechanisms of nuclear delivery of extracellular proteins are poorly understood, but involvement of importin-beta in this process is likely.[35,41] Recently, it was proposed that internalized EGF/EGFR complexes may leave endosomes at the nuclear-cytoplasmic interface and enter the nucleus *via* nuclear pores, implying the importin-beta complex.[42] Such a mechanism may also contribute to nuclear delivery of IGFBP-3, even though we have no direct evidence for such a scenario.

Nuclear functions of the insulin/IGF axis?

There is evidence that IGFBP-3 can interact both physically and functionally with transcription factors, such as RXR.[17] Thus, our finding that extracellular IGFBP-3 reaches the nucleus within 2–3 hr (Figs. 3–6), raises the possibility that nuclear IGFBP-3 may trigger rapid transcriptional changes (in

the receiving cell), due to its functional interaction with nuclear transcription factors. Consistent with this assumption, we found significant changes in the expression of several genes 6 hr after addition of IGFBP-3 to human diploid fibroblasts (L. Micutkova, unpublished). However, more work will be required to elucidate the precise molecular mechanism(s) by which nuclear uptake of IGFBP-3 leads to changes in the expression of these genes. It is interesting to note that other components of the insulin/IGF signaling pathway were described as targets for nuclear import. Thus, insulin receptor substrate-1 (IRS1)[43] and insulin receptor substrate-2[44] translocate to the nucleus, and recent data suggest that the IGF receptor I can also translocate to the nucleus, in response to site specific sumoylation.[45] IRS1 was also shown to interact with caveolin,[46] resulting in mutual stabilization of both proteins.[47]

Although these data suggest that the components of the insulin/IGF pathway have the potential for regulating nuclear function, the role of IGFBP-3 in this scenario remains to be further characterized. To summarize, we here show that extracellular IGFBP-3 is indeed translocated to the cell nucleus following well-described endocytic pathways, whereas the observed nuclear import mechanisms have to be further elucidated. Our findings provide a basis for identifying new regulators (*e.g.*, IGFBP-3 receptors, or endosomal proteins) of IGFBP-3 uptake and nuclear delivery, aiming to better understand the ability of extracellular IGFBP-3 to suppress tumor progression in epithelial cancers.

Acknowledgements

The authors acknowledge excellent technical support by Michael Neuhaus, Hans-Peter Viertler and Karin Gutleben. Work in P.J.D.'s laboratory was supported by grants from the Austrian Science Funds (NFN S93 and SFB021) and the EU (Integrated Project PROTEOMAGE). Work in the Huber laboratory was supported by the Austrian Science Funds (SFB021). Grant support to W. Zwerschke was from the European Union INCA project LSHC-CT-2005-018704 and BMBWK (BMBWK-651.048/0001-VI/2/2006). M.W.H. was supported by grants from the Austrian Science Funds (P19486-B12) and Austrian National Bank Jubiläumsfonds (P-11050). M.O. was supported by the grant from the Austrian Science Fund (FWF) P184468-B12.

References

1. Valentinis B, Baserga R. IGF-I receptor signalling in transformation and differentiation. *Mol Pathol* 2001;54:133–7.
2. Jones JI, Clemmons DR. Insulin-like growth factors and their binding proteins: biological actions. *Endocr Rev* 1995;16:3–34.
3. Kurmasheva RT, Houghton PJ. IGF-I mediated survival pathways in normal and malignant cells. *Biochim Biophys Acta* 2006;1766:1–22.
4. Firth SM, Baxter RC. Cellular actions of the insulin-like growth factor binding proteins. *Endocr Rev* 2002;23:824–54.
5. Yamada PM, Lee KW. Perspectives in Mammalian IGFBP-3 Biology: Local vs. Systemic Action. *Am J Physiol Cell Physiol* 2009;296:C954–76.
6. Buckbinder L, Talbott R, Velascomiguel S, Takenaka I, Faha B, Seizinger BR, Kley N. Induction of the growth inhibitor IGF-binding protein 3 by p53. *Nature* 1995;377:646–49.
7. Rajah R, Valentinis B, Cohen P. Insulin like growth factor (IGF)-binding protein-3 induces apoptosis and mediates the effects of transforming growth factor-beta 1 on programmed cell death through a p53- and IGF-independent mechanism. *J Biol Chem* 1997;272:12181–88.
8. Mannhardt B, Weinzimer SA, Wagner M, Fiedler M, Cohen P, Jansen-Durr P, Zwerschke W. Human papillomavirus type 16 E7 oncoprotein binds and inactivates growth-inhibitory insulin-like growth factor binding protein 3. *Mol Cell Biol* 2000;20:6483–95.
9. Santer FR, Moser B, Spoden GA, Jansen-Durr P, Zwerschke W. Human papillomavirus type 16 E7 oncoprotein inhibits apoptosis mediated by nuclear insulin-like growth factor binding protein-3 by inducing its ubiquitin/proteasome-dependent degradation. *Carcinogenesis* 2007;28:2511–20.
10. Santer FR, Bacher N, Moser B, Morandell D, Ressler S, Firth SM, Spoden GA, Sergi C, Baxter RC, Jansen-Durr P, Zwerschke W. Nuclear insulin-like growth factor binding protein-3 induces apoptosis and is targeted to ubiquitin/proteasome-dependent proteolysis. *Cancer Res* 2006;66:3024–33.
11. Hampel OZ, Kattan MW, Yang G, Haidacher SJ, Saleh GY, Thompson TC, Wheeler TM, Marcelli M. Quantitative immunohistochemical analysis of insulin-like growth factor binding protein-3 in human prostatic adenocarcinoma: a prognostic study. *J Urol* 1998;159:2220–5.
12. Hong J, Zhang G, Dong F, Rechler MM. Insulin-like growth factor (IGF)-binding protein-3 mutants that do not bind IGF-I or IGF-II stimulate apoptosis in human prostate cancer cells. *J Biol Chem* 2002;277:10489–97.
13. Silha JV, Sheppard PC, Mishra S, Gui Y, Schwartz J, Dodd JG, Murphy LJ. Insulin-like growth factor (IGF) binding protein-3 attenuates prostate tumor growth by IGF-dependent and IGF-independent mechanisms. *Endocrinology* 2006;147:2112–21.
14. Cohen P. Insulin-like growth factor binding protein-3: insulin-like growth factor independence comes of age. *Endocrinology* 2006;147:2109–11.
15. Schedlich LJ, Le Page SL, Firth SM, Briggs LJ, Jans DA, Baxter RC. Nuclear import of insulin-like growth factor-binding protein-3 and -5 is mediated by the importin beta subunit. *J Biol Chem* 2000;275:23462–70.
16. Jaques G, Noll K, Wegmann B, Witten S, Kogan E, Radulescu RT, Havemann K. Nuclear localization of insulin-like growth factor binding protein 3 in a lung cancer cell line. *Endocrinology* 1997;138:1767–70.
17. Liu B, Lee HY, Weinzimer SA, Powell DR, Clifford JL, Kurie JM, Cohen P. Direct functional interactions between insulin-like growth factor- binding protein-3 and retinoid X receptor-alpha regulate transcriptional signaling and apoptosis. *J Biol Chem* 2000;275:33607–13.
18. Cobb LJ, Mehta H, Cohen P. Enhancing the apoptotic potential of insulin-like growth factor-binding protein-3 in prostate cancer by modulation of CK2 phosphorylation. *Mol Endocrinol* 2009;23:1624–33.
19. Schedlich LJ, Young TF, Firth SM, Baxter RC. Insulin-like growth factor-binding protein (IGFBP)-3 and IGFBP-5 share a common nuclear transport pathway in T47D human breast carcinoma cells. *J Biol Chem* 1998;273:18347–52.
20. Lee KW, Liu B, Ma L, Li H, Bang P, Koeffler HP, Cohen P. Cellular internalization of insulin-like growth factor binding protein-3: distinct endocytic pathways facilitate re-uptake and nuclear localization. *J Biol Chem* 2004;279:469–76.

21. Pircher H, Matscheski A, Laich A, Hermann M, Moser B, Viertler HP, Micutkova L, Lindner H, Sarg B, Zwerschke W, Jansen-Durr P. A new method for the purification of bioactive insulin-like growth factor-binding protein-3. *Protein Expr Purif* 2010;71:160–7.
22. Cao H, Thompson HM, Krueger EW, McNiven MA. Disruption of Golgi structure and function in mammalian cells expressing a mutant dynamin. *J Cell Sci* 2000;113:1993–2002.
23. Hess MW, Muller M, Debbage PL, Vetterlein M, Pavelka M. Cryopreparation provides new insight into the effects of brefeldin A on the structure of the HepG2 Golgi apparatus. *J Struct Biol* 2000;130:63–72.
24. Robinson JM, Karnovsky MJ. Rapid-freezing cytochemistry: preservation of tubular lysosomes and enzyme activity. *J Histochem Cytochem* 1991;39:787–92.
25. van Donselaar E, Posthuma G, Zeuschner D, Humbel BM, Slot JW. Immunogold labeling of cryosections from high-pressure frozen cells. *Traffic* 2007;8:471–85.
26. Shah N, Zhang S, Harada S, Smith RM, Jarett L. Electron microscopic visualization of insulin translocation into the cytoplasm and nuclei of intact H35 hepatoma cells using covalently linked Nanogold-insulin. *Endocrinology* 1995;136:2825–35.
27. Jerome L, Alami N, Belanger S, Page V, Yu Q, Paterson J, Shiry L, Pegram M, Leyland-Jones B. Recombinant human insulin-like growth factor binding protein 3 inhibits growth of human epidermal growth factor receptor-2-overexpressing breast tumors and potentiates herceptin activity in vivo. *Cancer Res* 2006;66:7245–52.
28. Weinzimer SA, Gibson TB, Collett-Solberg PF, Khare A, Liu B, Cohen P. Transferrin is an insulin-like growth factor-binding protein-3 binding protein. *J Clin Endocrinol Metab* 2001;86:1806–13.
29. Hinrichsen L, Harborth J, Andrees L, Weber K, Ungewickell EJ. Effect of clathrin heavy chain- and alpha-adaptin-specific small inhibitory RNAs on endocytic accessory proteins and receptor trafficking in HeLa cells. *J Biol Chem* 2003;278:45160–70.
30. Drab M, Verkade P, Elger M, Kasper M, Lohn M, Lauterbach B, Menne J, Lindschau C, Mende F, Luft FC, Schedl A, Haller H, et al. Loss of caveolae, vascular dysfunction, and pulmonary defects in caveolin-1 gene-disrupted mice. *Science* 2001;293:2449–52.
31. Dharmawardhane S, Schurmann A, Sells MA, Chernoff J, Schmid SL, Bokoch GM. Regulation of macropinocytosis by p21-activated kinase-1. *Mol Biol Cell* 2000;11:3341–52.
32. Ungewickell EJ, Hinrichsen L. Endocytosis: clathrin-mediated membrane budding. *Curr Opin Cell Biol* 2007;19:417–25.
33. Shaner NC, Campbell RE, Steinbach PA, Giepmans BN, Palmer AE, Tsien RY. Improved monomeric red, orange and yellow fluorescent proteins derived from Discosoma sp. red fluorescent protein. *Nat Biotechnol* 2004;22:1567–72.
34. Rabut G, Doye V, Ellenberg J. Mapping the dynamic organization of the nuclear pore complex inside single living cells. *Nat Cell Biol* 2004;6:1114–21.
35. Wagstaff KM, Jans DA. Importins and beyond: non-conventional nuclear transport mechanisms. *Traffic* 2009;10:1188–98.
36. Kutay U, Izaurralde E, Bischoff FR, Mattaj IW, Gorlich D. Dominant-negative mutants of importin-beta block multiple pathways of import and export through the nuclear pore complex. *EMBO J* 1997;16:1153–63.
37. Jurgeit A, Berlato C, Obrist P, Ploner C, Massoner P, Schmölzer J, Haffner MC, Klocker H, Huber LA, Geley S, Doppler W. Insulin-like growth factor-binding protein-5 enters vesicular structures but not the nucleus. *Traffic* 2007;8:1815–28.
38. Butt AJ, Dickson KA, McDougall F, Baxter RC. Insulin-like growth factor-binding protein-5 inhibits the growth of human breast cancer cells in vitro and in vivo. *J Biol Chem* 2003;278:29676–85.
39. Doherty GJ, McMahon HT. Mechanisms of endocytosis. *Annu Rev Biochem* 2009;78:857–902.
40. Leal SM, Liu Q, Huang SS, Huang JS. The type V transforming growth factor beta receptor is the putative insulin-like growth factor-binding protein 3 receptor. *J Biol Chem* 1997;272:20572–6.
41. Carpenter G, Liao HJ. Trafficking of receptor tyrosine kinases to the nucleus. *Exp Cell Res* 2009;315:1556–66.
42. Wang YN, Yamaguchi H, Huo L, Du Y, Lee HJ, Lee HH, Wang H, Hsu JM, Hung MC. The translocon SEC61{beta} localized in the inner nuclear membrane transports membrane-embedded EGF receptor to the nucleus. *J Biol Chem* 2010;285:38720–9.
43. Prisco M, Santini F, Baffa R, Liu M, Drakas R, Wu A, Baserga R. Nuclear translocation of insulin receptor substrate-1 by the simian virus 40 T antigen and the activated type 1 insulin-like growth factor receptor. *J Biol Chem* 2002;277:32078–85.
44. Sun H, Tu X, Prisco M, Wu A, Casiburi I, Baserga R. Insulin-like growth factor I receptor signaling and nuclear translocation of insulin receptor substrates 1 and 2. *Mol Endocrinol* 2003;17:472–86.
45. Sehat B, Tofigh A, Lin Y, Trocmé E, Liljedahl U, Lagergren J, Larsson O. SUMOylation mediates the nuclear translocation and signaling of the IGF-1 receptor. *Sci Signal* 2010;3:ra10.
46. Panetta D, Biedi C, Repetto S, Cordera R, Maggi D. IGF-I regulates caveolin 1 and IRS1 interaction in caveolae. *Biochem Biophys Res Commun* 2004;316:240–3.
47. Chen J, Capozza F, Wu A, Deangelis T, Sun H, Lisanti M, Baserga R. Regulation of insulin receptor substrate-1 expression levels by caveolin-1. *J Cell Physiol* 2008;217:281–9.